

Multistability and High Codimension Bifurcations in Synergistic Epidemics on Heterogeneous Networks

Francisco J. Pérez-Reche¹ and Sergei N. Taraskin²

¹*School of Natural and Computing Sciences, University of Aberdeen, Aberdeen, UK**

²*St. Catharine's College and Department of Chemistry, University of Cambridge, Cambridge, UK†*

We investigate the impact of network heterogeneity on synergistic contagion dynamics. By extending a synergistic contagion model to diverse heterogeneous network topologies, we uncover the emergence of novel dynamical regimes characterized by multiple stable states, separated by a rich set of bifurcations reaching up to codimension 4. Additionally, we demonstrate how synergy fundamentally reshapes the influence of nodes based on their degree. Unlike in non-synergistic epidemics, low-degree nodes can play a pivotal role in enabling network invasion at the onset of spread, while high-degree nodes can trigger explosive contagion. These findings challenge conventional control strategies, highlighting the need for new approaches to enhance or suppress synergistic contagion.

Network models have emerged as an indispensable framework for describing the dynamics of complex systems composed of interacting units [1–3]. These models have been widely applied to a variety of natural and artificial processes, including the spread of infections, information, products, and malware [4–6]. In particular, compartmental epidemic models on networks have provided valuable insight into epidemic invasion thresholds, the design of effective immunization strategies, and the impact of network structure on overall dynamics [4, 7].

Traditional compartmental epidemic models assume that the infection transmission rate, α , between an infected-susceptible pair is independent of the states of other neighboring nodes [4]. Such models predict two possible infection regimes: (I) a disease-free regime when $\alpha < \alpha_c$, and (II) an epidemic regime when $\alpha > \alpha_c$. Although the critical transmission rate at the invasion threshold, α_c , varies depending on the structure of the network, the transition between these two regimes remains continuous regardless of the topology of the network.

Pairwise interactions are often insufficient to capture the complexity of real-world dynamics. Accurate modeling of processes such as infection transmission [8], biological invasions [9, 10], and social contagion [11, 12] requires higher-order interactions involving groups of more than two nodes. Theoretical frameworks incorporating such interactions include threshold models [13–19], generalized epidemic models with memory [19–23], contagion on simplicial complexes [24, 25], and synergistic epidemic models [26–33]. These models often reveal a third regime (III) at intermediate values of α , where disease-free and epidemic states can coexist [15–19, 24, 25, 29–33]. In this regime, the likelihood of an epidemic is sensitive to the initial conditions of infection and explosive contagion can occur.

The observation of three distinct dynamical regimes (I–III) appears to be robust in the existing literature, emerging across various spreading processes, higher-order interactions, and network topologies. This raises the intriguing conjecture that three regimes may be a characteristic feature of synergistic spread on any network, just as two regimes (I and II) universally describe non-synergistic spread.

Here, we show that synergistic epidemics on heterogeneous networks can exhibit more than three distinct dynamical regimes, highlighting the complex interplay between network topology and contagion. Identifying these regimes advances our understanding of complex epidemic behavior in real-world systems where synergy and heterogeneity are ubiquitous.

The model. The model proposed in Ref. [31] for SIS synergistic epidemics spreading in random regular graphs is extended here to accommodate epidemics spreading in networks with arbitrary node degree distribution. The nodes of the network can be either infected or susceptible. In a time interval δt , infected individuals can recover and become susceptible with probability $\mu\delta t$. Assuming that each of the n infected neighbors of a susceptible node transmits the infection independently with the rate λ_n , the probability of infection can be expressed as $\Lambda_n\delta t = 1 - (1 - \lambda_n\delta t)^n$.

Synergistic transmission is captured through an explicit dependence of λ_n on the number of infected neighbors of the recipient node. Following Refs. [29, 31], we consider the S-synergy associated with synergistic effects between the susceptible neighbors of the recipient node. For instance, this concept is relevant to the spread of social content [29]. Specifically, we assume $\lambda_n = \min\{\alpha e^{\beta(k-n)}, 1/\delta t\}$, where k is the node degree of the recipient node. The parameter α represents the

intrinsic transmission rate between an isolated infected-susceptible pair, while β controls the degree of synergistic opposition ($\beta < 0$) or reinforcement ($\beta > 0$) of transmission by susceptible neighbors.

To study the impact of network heterogeneity on synergistic epidemics, we analyse model and real networks. As model networks, we considered three distinct types of random graphs that span a range of degree heterogeneity: Erdos-Renyi (ER), binary (BG), and power-law (PL) networks, each characterized by different node degree distributions:

$$\rho_k = \begin{cases} \frac{\langle k \rangle^k e^{-\langle k \rangle}}{k!} & : \text{ER}(\langle k \rangle), \\ \varphi \delta_{kk_1} + (1 - \varphi) \delta_{kk_2} & : \text{BG}(k_1, k_2, \varphi), \\ \frac{k^{-m}}{A}, k \in [k_{\min}, k_{\max}] & : \text{PL}(k_{\min}, k_{\max}, m). \end{cases} \quad (1)$$

Here, $\delta_{kk'}$ denotes the Kronecker delta, $A = \sum_{k=k_{\min}}^{k_{\max}} k^{-m}$ is a normalization factor, and $\langle k \rangle$ is the mean node degree. For real networks, we analysed the Douban social network [34] and the Western US power grid [35].

Our model can describe both continuous ($\delta t \rightarrow 0$) and discrete-time dynamics (finite δt) with the results mainly presented for the latter which encompasses all the effects observed for continuous dynamics (see Figs. 2(a) and 4(a) in [36] for continuous-time examples). Specifically, we set $\delta t = 1$ so that $\alpha \in [0, 1]$ becomes an intrinsic transmission probability. Within this framework, the spreading dynamics depends on a set of parameters $\Gamma = \{\alpha, \beta, \mu, \Gamma_N\}$, where the set Γ_N describes the node degree distribution (e.g. $\Gamma_N = \{k_1, k_2, \varphi\}$ for a binary graph).

We studied the model in the long-time limit ($t \rightarrow \infty$), which determines whether the network is vulnerable to spread of infection or not. To gain mathematical insight, a single-site heterogeneous mean-field (SSHMF) approximation was employed. The SSHMF ignores dynamical correlations between the states of connected nodes and assumes that the probability that a node is infected only depends on its degree k [4, 6]. The results obtained by this approach are qualitatively consistent with Monte Carlo simulations of the exact model, which we run on networks constructed with the uncorrelated configuration model [1, 37] (see results in [36]).

SSHMF approximation. Within the SSHMF, the probability $p_k(t; \Gamma)$ that a node with k neighbours is in-

fectured is the solution of the following equation:

$$p_k(t+1; \Gamma) = (1 - \mu)p_k(t; \Gamma) + (1 - p_k(t; \Gamma))q_k(\theta), \quad (2)$$

where

$$q_k(\theta) = \sum_{n=1}^k \binom{k}{n} \Lambda_n \theta^n (1 - \theta)^{k-n}, \quad (3)$$

is the rate at which a susceptible node with k neighbours becomes infected. This rate depends on the probability

$$\theta = \frac{\langle k p_k \rangle}{\langle k \rangle}, \quad (4)$$

that any given neighbour of the recipient node is infected. Here, $\langle \cdot \rangle$ denotes the average over the node degree distribution.

The predictions of the model for p_k in the long-time limit correspond to the fixed points of Eq. (2) which gives

$$p_k^\infty(\Gamma) \equiv \lim_{t \rightarrow \infty} p_k(t; \Gamma) = f_k(\theta, \Gamma) \equiv \frac{q_k(\theta)}{\mu + q_k(\theta)}, \quad (5)$$

with θ being the zeros of the following function (cf. Eq. (4)):

$$F(\theta; \Gamma) = -\theta + \frac{\langle k f_k(\theta) \rangle}{\langle k \rangle}. \quad (6)$$

A fixed point at θ_* is stable if $\partial_\theta F(\theta; \Gamma)|_{\theta=\theta_*} < 0$. The infection-free state with $\theta_* = 0$ is always a fixed point since $F(0; \Gamma) = 0$ for any Γ . Additionally, for the networks considered here, $F(\theta; \Gamma)$ can have up to four positive zeros. Consequently, the long-time behaviour of the model can fall into five different regimes (Fig. 1) distinguished by the total number of fixed points. Regime I represents an infection-free stable state characterized by $\theta_* = 0$. In regimes II-V, there is at least one stable fixed point located at $\theta_* > 0$, corresponding to endemic infection. In regimes III and V, both the infection-free and endemic states are stable. In regimes IV and V, two stable endemic states are possible depending on the initial conditions.

Variation in the model parameters can induce transitions between regimes, which are associated with bifurcations where the number of fixed points changes. A codimension- \bar{d} bifurcation occurs at $\theta = \theta_* \in [0, 1]$ if a non-empty set, $\mathcal{B}_{\bar{d}}^s(\theta_*)$, of parameters exists, defined as follows:

$$\mathcal{B}_{\bar{d}}^s(\theta_*) = \left\{ \Gamma \left| F(\theta_*, \Gamma) = 0, \{F^{(l)}(\theta_*, \Gamma) = 0\}_{l=1}^{\bar{d}}, F^{(\bar{d}+1)}(\theta_*, \Gamma) \neq 0 \right. \right\}. \quad (7)$$

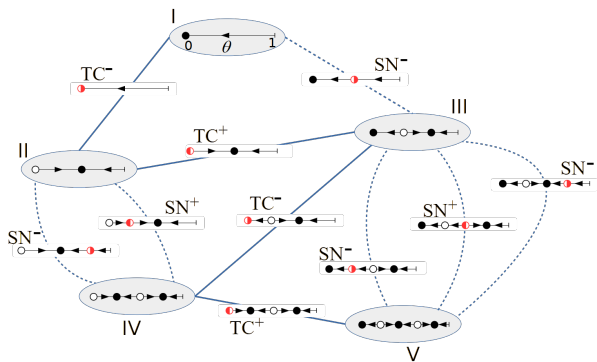


FIG. 1: Graph representation of the five observed dynamical regimes (nodes represented by ellipses) and the codimension-1 bifurcations connecting them (solid and dashed links for $TC^\pm = \mathcal{B}_1^\pm(0)$ and $SN^\pm = \mathcal{B}_1^\pm(\theta_*)$, respectively). Flow diagrams illustrate the dynamics of θ , with arrows indicating evolution toward stable (●) or away from unstable (○) fixed points. Bifurcation points are marked by half-filled circles: ● for negative and ○ for positive bifurcations.

Here, $F^{(l)}(\theta_*; \Gamma)$ denotes the l -th derivative of F with respect to θ , evaluated at θ_* , and $s = \text{sign}(F^{(\bar{d}+1)}(\theta_*; \Gamma))$. The codimension \bar{d} is the minimum number of parameters that must be varied for the bifurcation to occur [38].

For the heterogeneous networks studied here, we observed bifurcations up to codimension-4 that connect the long-time regimes I-V. Specifically, Fig. 1 illustrates transitions associated with codimension-1 bifurcations. Non-synergistic epidemics ($\beta = 0$) can only exhibit regimes I and II irrespective of the node degree distribution (see Sec. I in [36]). Regimes I and II are connected by a transcritical bifurcation, $TC^- = \mathcal{B}_1^-(0)$, which drives the well-known continuous transition between infection-free and endemic states.

For synergistic epidemics on regular graphs, a discontinuous transition between regimes I and III can occur, driven by a saddle-node bifurcation, $SN^- \equiv \mathcal{B}_1^-(\theta_*)$, located at $\theta_* \in (0, 1)$ [31]. The TC^- and SN^- bifurcations collide at a codimension-2 saddle-node-transcritical bifurcation, $SNT^- \equiv \mathcal{B}_2^-(0)$.

Codimension-1 and 2 bifurcations in heterogeneous networks. In contrast to regular graphs, the synergistic spread in heterogeneous networks can exhibit multiple SNT bifurcations. This phenomenon, which can be observed for all the network types studied here, is illustrated by the bifurcation diagram in (μ, φ) parameter space for binary graphs $BG(10, 30, \varphi)$ shown in Fig. 2(a) (see examples for ER, PL and real networks in [36]).

Fig. 2(b) shows a bifurcation diagram in the (α, β)

space for epidemics with $\mu = 0.1$ spreading on a $BG(10, 30, 0.6)$ which exhibit three SNT bifurcations. Depending on the values of α and β , the long-time behaviour of epidemics can fall into any of the five regimes I to V. As expected, for any β and sufficiently small α the epidemic does not spread. The specific regimes observed for intermediate values of α depend on the value of β . The insets in Fig. 2(b) show the expected proportion of infected nodes, $p = \langle p_k^\infty \rangle$, as a function of α for four different values of β . These invasion curves illustrate different ways to transition between infection-free and endemic regimes through codimension-1 bifurcations, corresponding to different paths in the graph of Fig. 1:

- (i): $\beta > \beta_{SNT_1^-}$: A classical smooth transition between regimes I and II occurs at a TC_1^- bifurcation as α increases.
- (ii): $\beta \in (\beta_{SNT_2^+}, \beta_{SNT_1^-})$: Three regimes, I-III, are possible. Increasing α from regime I leads to a discontinuous transition to regime II at TC_2^+ . Conversely, decreasing α from regime II results in a discontinuous transition back to regime I at SN_1^- . In regime III, the system can settle into either the infection-free or endemic state depending on initial conditions, as illustrated by the basins of attraction in Fig. 2(b).
- (iii): $\beta \in (\beta_{SNT_3^-}, \beta_{SNT_2^+})$: Regimes I-IV can be observed. As α increases from regime I, p initially rises smoothly at TC_3^- , followed by a discontinuous jump to regime II at SN_2^+ . Decreasing α from regime II leads to a discontinuous transition back to regime I at SN_1^- .
- (iv): $\beta < \beta_{SNT_3^-}$: The regime transition sequence I-III-V-IV-II is observed as α increases. These regimes are separated by the sequence of bifurcations, SN_1^- , SN_3^- , TC_4^+ , and SN_2^+ . Increasing α from regime I leads to two discontinuities in p , separated by an interval of smooth variation corresponding to endemic states with infection levels lower than those in regime II. As in case (iii), decreasing α results in a discontinuous transition back to regime I at SN_1^- .

In addition to SNT bifurcations, synergistic epidemics in heterogeneous networks can exhibit codimension-2 cusp bifurcations, denoted as $C^\pm \equiv \mathcal{B}_2^\pm(\theta_*)$, which occur for $\theta_* \in (0, 1)$ and result from the SN^+ - SN^- interaction. Fig. 2(c) presents a bifurcation diagram for a binary graph $BG(10, 30, 0.82)$, displaying two codimension-2 bifurcations: SNT_1^- and cusp C^+ . When $\beta > \beta_{C^+}$, varying α at fixed β leads to transitions between regimes I and II through the codimension-1 bifurcations previously described, following regime sequences of type (i) or (ii). In contrast,

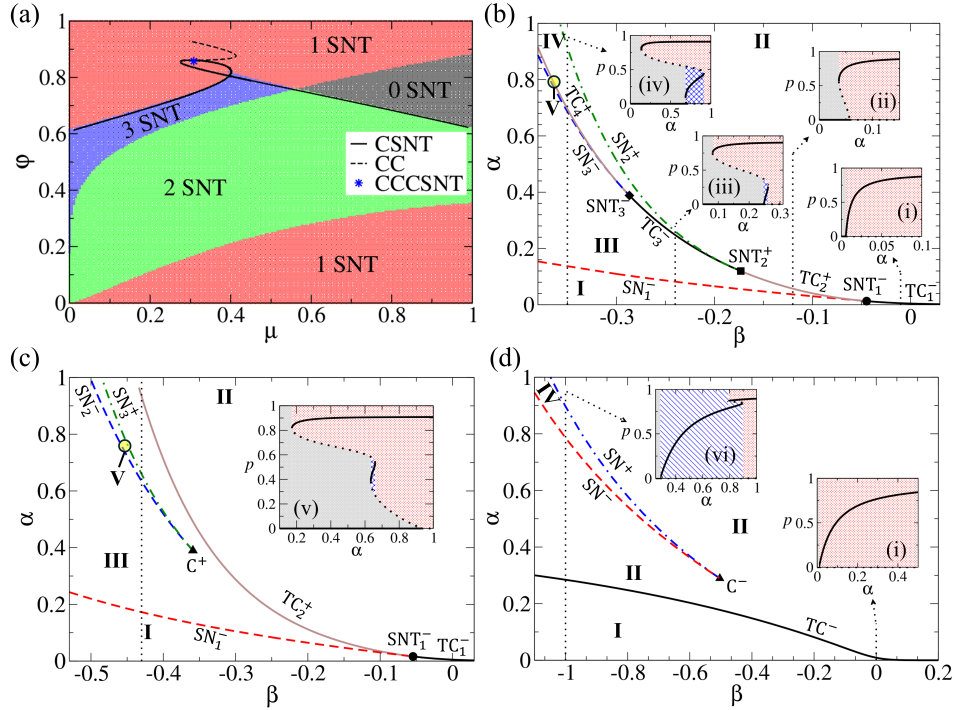


FIG. 2: Bifurcation diagrams and the mean proportion p of infected nodes in synergistic SIS epidemics. (a) Codimension-4 bifurcation (CCCSNT⁻, star) in BG(10, 30, φ), projected onto the (μ, φ) plane at $(\alpha, \beta, \mu, \varphi) = (0.096, -0.104, 0.298, 0.861)$. Codimension-3 bifurcations (CSNT, CC) are shown as solid and dashed lines, respectively. Colors indicate regions with different numbers of codimension-2 SNT bifurcations. (b,c) Bifurcations in the (α, β) plane for $\mu = 0.1$ on BG(10, 30, φ) with $\varphi = 0.6$ and 0.76 , respectively. Regimes I–V are identified and invasion curves $p(\alpha)$ for regime transitions (i)–(v) are shown in the insets. Stable/unstable states shown with solid/dashed lines. Shaded regions represent basins of attraction: grey (infection-free), blue dashed (low-endemic), red dotted (high-endemic). (d) Analogous results for $\mu = 0.1$ on PL(2, 50, 2) graphs; insets show transitions (i) and (vi). In (b)–(d), codimension-1 bifurcations of TC and SN type are indicated by continuous and dashed lines, respectively.

(v): if $\beta < \beta_{C^+}$, the system can fall sequentially into regimes I–III–V–III–II separated by the sequence of bifurcations, SN⁻, SN⁻, SN⁺ and TC⁺ (inset in Fig. 2(c)). In this case, all transitions between different regimes are discontinuous.

A codimension-2 bifurcation of type C⁻ can also exist without SNT bifurcations, thus yielding a qualitatively distinct bifurcation diagram, as illustrated in Fig. 2(d) for PL networks; similar results for real networks are shown in [36]. When $\beta > \beta_{C^-}$, regimes I and II are connected by a smooth transition associated with a TC⁻ bifurcation, resembling case (i) described above. In contrast,

(vi): if $\beta < \beta_{C^-}$, the regime sequence I–II–IV–II can be observed (see inset in Fig. 2(d)). Increasing α from regime I at constant β leads to a gradual increase in p at TC⁻, followed by a discontinuous transition to regime II at SN⁺. In contrast, decreasing α from

regime II results in a discontinuous drop in p at SN⁻, followed by a smooth decrease toward regime I.

Codimension-3 and 4 bifurcations in heterogeneous networks. Codimension-3 bifurcations of type $\mathcal{B}_3^\pm(0)$ can occur for epidemics spreading on binary, ER, PL graphs and real networks. These bifurcations arise from the interaction of C and SNT bifurcations, and are referred to as cusp-(saddle-node-transcritical) (CSNT) bifurcations. The solid curve in Fig. 2(a) shows the locus of such bifurcations in the space (μ, φ) for epidemics spreading on BG(10, 30, φ) graphs.

When crossing a CSNT⁻ bifurcation by increasing α , the proportion of infected nodes, p , increases smoothly, resembling the behaviour observed when crossing TC₁⁻ in case (i) described above (see Fig. 1(e) in [36]). Crossing a CSNT⁺ bifurcation by increasing α results in a discontinuous jump in p , analogous to the behaviour seen when

crossing TC_2^+ in case (ii) (see Fig. 1(d) in [36]).

The only bifurcation of codimension-3 observed at $\theta_* \in (0, 1)$ is of type $\mathcal{B}_3^-(\theta_*)$, and it occurs for epidemics spreading on binary graphs. These bifurcations, referred to as cusp-cusp (CC^-) bifurcations, result from the merging of two cusp bifurcations. For $BG(10, 30, \varphi)$, they are located along the dashed line shown in Fig. 2(a). When crossing a CC^- bifurcation by decreasing α , p exhibits a discontinuous drop from regime III to regime I, analogous to the behaviour observed when crossing a SN^- bifurcation in cases (ii)-(v) (see Figs. 1(b)-(c) in [36]).

A single codimension-4 bifurcation was identified in the networks studied: a $\mathcal{B}_4^-(0)$ bifurcation termed a (cusp-cusp)-(cusp-saddle-node-transcritical) ($CCCSNT^-$) bifurcation. This bifurcation results from the interaction between $CSNT^+$ and CC^- bifurcations. The $CCCSNT^-$ bifurcation occurs in epidemics spreading on binary graphs with only a specific choice of parameters $(\alpha, \beta, \mu, \varphi)$ (see the star symbol in Fig. 2(a)). Crossing the $CCCSNT^-$ bifurcation by increasing α leads to a smooth transition between regimes I and II (see Fig. 1(a) in [36]). No codimension-4 bifurcations were observed for epidemics spreading in other studied networks.

Heterogeneous infection. For non-synergistic epidemics on heterogeneous networks, it is well established that the transition between disease-free regime I and endemic regime II is primarily driven by the infection of high-degree nodes [4]. Fig. 3(a) illustrates this for non-synergistic epidemics spreading on a PL network. When increasing α and crossing the TC^- bifurcation, the system smoothly enters regime II. The average degree of infected nodes, $\bar{k}_{\text{inf}} = \sum_k k p_k^\infty / \sum_k p_k^\infty$, decreases monotonically as nodes with a lower degree become more likely to be infected (see p_k^∞ in the insets). A similar pattern holds for synergistic epidemics with $\beta > 0$.

In contrast, negative synergy ($\beta < 0$) leads to qualitatively different dynamics, shown in Fig. 3(b). Here, lower-degree nodes are more easily infected, and \bar{k}_{inf} increases with α . More notably, abrupt transitions in infection levels occur as high-degree nodes suddenly switch between susceptible and infected states, corresponding to the SN^\pm bifurcations. The insets show p_k^∞ distributions for low- (green) and high- (red) endemic states, with unstable distributions in blue. Similar examples of p_k^∞ distributions for PL networks are shown in Fig. 9 of [36].

Conclusions. We have demonstrated that the combination of network heterogeneity and synergistic effects in epidemics can produce far more complex dynamics than those found in non-synergistic models or synergistic epidemics on homogeneous networks. Using a single-site mean-field approach, supported by exact numerical

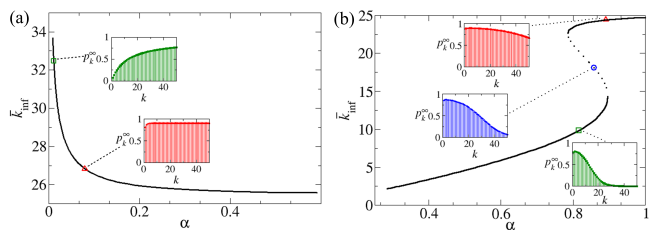


FIG. 3: Mean degree of infected nodes \bar{k}_{inf} vs. α in SIS epidemics with $\mu = 0.1$ on $PL(1, 50, 2)$ graphs. (a) Non-synergistic case ($\beta = 0$), corresponding to invasion curve (i) in Fig. 2. (b) Synergistic case ($\beta = -1$), corresponding to curve (iv) in the same figure. Insets show the infection probability distribution p_k^∞ at selected α values.

simulations, we identified five distinct long-term regimes linked by bifurcations of up to codimension four. Notably, the emergence of regimes IV and V allows for two stable low- and high-endemic states, a phenomenon previously unreported in this class of models. Such regimes have been observed in threshold models, but only with heterogeneous susceptibility of the nodes [22].

Our results reveal the contrasting roles of high- and low-degree nodes in epidemics with negative synergy ($\beta < 0$), where susceptible neighbors inhibit transmission. In contrast to non-synergistic spread—where high-degree nodes drive endemicity—low-degree nodes here sustain infections as α increases, while high-degree nodes are responsible for abrupt changes in prevalence. This underscores the counterintuitive effects of synergy on epidemic thresholds and informs the design of adaptive control strategies.

The model studied here is a special case of a broader class of models for spreading processes for which the mean proportion of infected nodes p changes over time with the rate $R(p)$ obeying the following properties: (i) $R(0) = 0$, ensuring p remains unchanged in the absence of infection, and (ii) $R(1) < 1$, guaranteeing that a fully infected system is unstable due to recovery. Nonlinearities in R can give rise to multiple quasi-stationary regimes with $R = 0$ and complex bifurcation diagrams. In synergistic epidemics on networks, we have shown that these emerge from the interplay between network heterogeneity and transmission dynamics. More broadly, we expect such phenomena to be widespread in systems with high-order interactions between nodes leading to nonlinear $R(p)$.

F.J.P.R. acknowledges funding from BBSRC (grant no. BB/Y513027/1).

-
- * fperez-reche@abdn.ac.uk
† snt1000@cam.ac.uk
- [1] M. E. J. Newman, *Networks: an introduction* (Oxford University Press, Oxford, 2010).
 - [2] A. Barrat, M. Barthélemy, and A. Vespignani, *Dynamical Processes on Complex Networks* (Cambridge University Press, Cambridge, 2008).
 - [3] S. N. Dorogovtsev and J. F. F. Mendes, *The nature of complex networks* (Oxford University Press, Oxford, 2022).
 - [4] R. Pastor-Satorras, C. Castellano, P. Van Mieghem, and A. Vespignani, *Reviews of Modern Physics* **87**, 925 (2015).
 - [5] C. Castellano, S. Fortunato, and V. Loreto, *Rev. Mod. Phys.* **81**, 591 (2009).
 - [6] J. P. Gleeson, *Physical Review X* **3**, 021004 (2013).
 - [7] P. Clusella, P. Grassberger, F. J. Pérez-Reche, and A. Politi, *Physical Review Letters* **117**, 208301 (2016).
 - [8] M. J. Silk, M. Q. Wilber, and N. H. Fefferman, *Ecology Letters* **25**, 2217 (2022).
 - [9] J. J. Ludlam, G. J. Gibson, W. Otten, and C. A. Gilligan, *J. R. Soc. Interface* **9**, 949 (2011).
 - [10] D. M. Gordon, *Ant encounters* (Princeton University Press, Princeton, 2010).
 - [11] D. Centola, J. Becker, D. Brackbill, and A. Baronchelli, *Science* **360**, 1116 (2018).
 - [12] N. O. Hodas and K. Lerman, *Scientific Reports* 2014 4:1 **4**, 1 (2014).
 - [13] M. Granovetter, *American Journal of Sociology* **83**, 1420 (1978).
 - [14] D. Watts, *PNAS* **99**, 5766 (2002).
 - [15] H. Chae, S.-H. Yook, and Y. Kim, *New Journal of Physics* **17**, 23039 (2015).
 - [16] B. Min and M. San Miguel, *Scientific Reports* 2018 8:1 **8**, 1 (2018).
 - [17] J. Kook, J. Choi, and B. Min, *Physical Review E* **104**, 044306 (2021).
 - [18] J. P. Gleeson and D. J. Cahalane, *Physical Review E* **75**, 056103 (2007).
 - [19] J. C. Miller, *Physical Review E* **94**, 032313 (2016).
 - [20] H.-K. Janssen, M. Müller, and O. Stenull, *Physical Review E* **70**, 026114 (2004).
 - [21] P. S. Dodds and D. J. Watts, *Physical Review Letters* **92**, 218701 (2004).
 - [22] P. S. Dodds and D. J. Watts, *Journal of theoretical biology* **232**, 587 (2005).
 - [23] G. Bizhani, M. Paczuski, and P. Grassberger, *Phys. Rev. E* **86**, 11128 (2012).
 - [24] I. Iacopini, G. Petri, A. Barrat, and V. Latora, *Nature Communications* 2019 10:1 **10**, 1 (2019).
 - [25] J. T. Matamalas, S. Gómez, and A. Arenas, *Physical Review Research* **2**, 012049 (2020).
 - [26] F. J. Pérez-Reche, J. J. Ludlam, S. N. Taraskin, and C. A. Gilligan, *Physical Review Letters* **106**, 218701 (2011).
 - [27] D. Broder-Rodgers, F. J. Pérez-Reche, and S. N. Taraskin, *Physical Review E* **92**, 062814 (2015).
 - [28] S. N. Taraskin and F. J. Pérez-Reche, *Physical Review E* **88**, 062815 (2013).
 - [29] J. Gómez-Gardeñes, L. Lotero, S. N. Taraskin, and F. J. Pérez-Reche, *Scientific reports* **6**, 19767 (2016).
 - [30] Q.-H. Liu, W. Wang, M. Tang, T. Zhou, and Y.-C. Lai, *Physical Review E* **95**, 042320 (2017).
 - [31] S. N. Taraskin and F. J. Pérez-Reche, *Journal of Physics A: Mathematical and Theoretical* **52**, 195101 (2019).
 - [32] V. R. V. Assis and M. Copelli, *Phys. Rev. E* **80**, 61105 (2009).
 - [33] C. Lin, Z. Yan, J. Gao, and J. Xiao, *Journal of Physics A: Mathematical and Theoretical* **56**, 215001 (2023).
 - [34] J. Kunegis, in *Proc. Int. Conf. on World Wide Web Companion* (2013) pp. 1343–1350.
 - [35] R. A. Rossi and N. K. Ahmed, in *AAAI* (2015) pp. 4292–4293.
 - [36] See Supplemental Material.
 - [37] M. Catanzaro, M. Boguñá, and R. Pastor-Satorras, *Physical Review E - Statistical, Nonlinear, and Soft Matter Physics* **71**, 10.1103/PhysRevE.71.027103 (2005).
 - [38] S. H. Strogatz, *Nonlinear Dynamics and Chaos* (Addison-Wesley, Reading, Massachusetts, 1994).